Electronic Supplementary Material (ESI) for Journal of Materials Chemistry C.

SUPPORTING INFORMATION

Supporting Information

Structural parameters versus third order optical susceptibility of Zinc porphyrin molecules

Amina Yasin, Vijayakumar S. Nair, Mohd Hasbi Ab-Rahim, Yoshihisa Yamaoka, Chandra S. Yelleswarapu*, Rajan Jose*

Synthetic scheme of the Por-C_n-RA_m molecules

The Por-C_n-RA_m series of molecules were synthesized through a strategy as explained briefly in Scheme S1, however the details of their synthesis and characterizations are explained in our recent published article.[1]

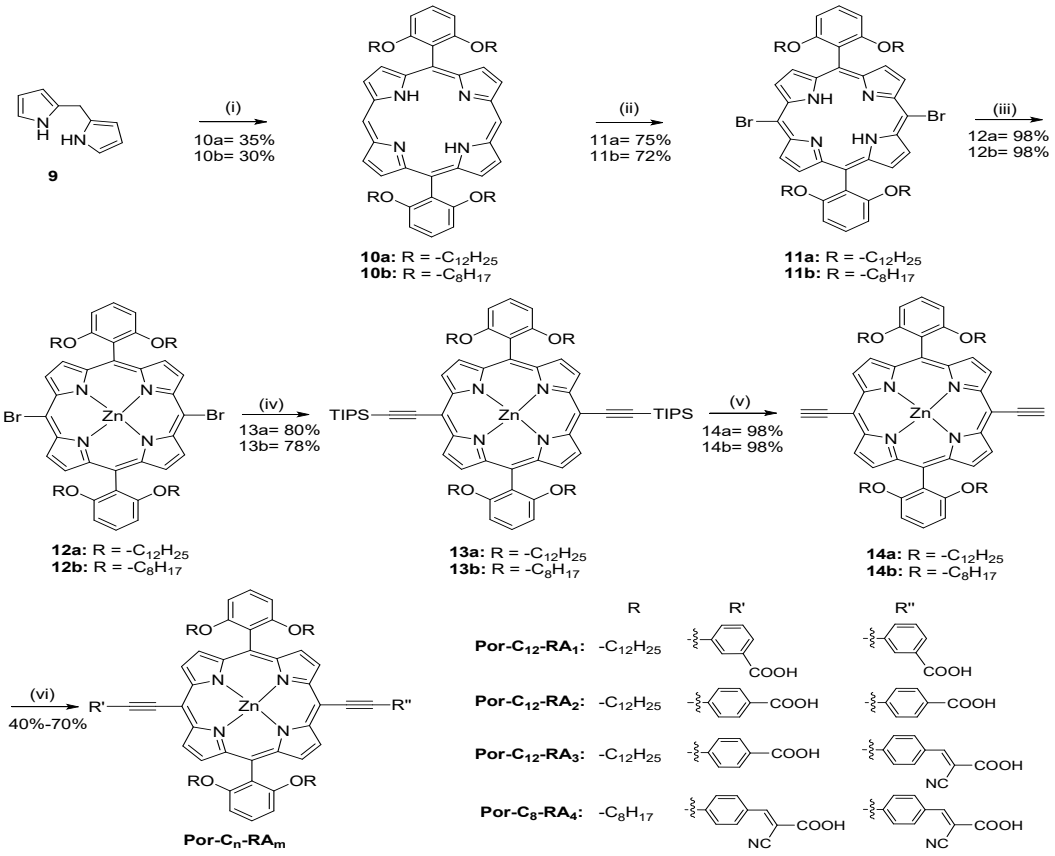

Scheme S1. Reagents: (i) a) 6, TFA, DCM, N_2, 23 °C, 4 hr; b) DDQ, 1 hr; (ii) NBS, DCM, N_2, 6 hr; (iii) $Zn(OAc)_2.2H_2O$, DCM, CH_3OH, 23 °C, 24 hr; (iv) TIPS-acetylene, THF, CuI, $Pd(PPh_3)_2Cl_2$, NEt_3, N_2, 85 °C, 8hr; (v) TBAF, THF, N_2, 6hr; (vi) various substituted phenyl iodide, THF, NEt_3, $Pd_2(dba)_3$, $AsPh_3$, N_2, 85 °C, 5hr.

General synthetic procedure of Por-C_n-RA_m porphyrins: To a degassed solution of compound 12 and 14 (1 mmol) and various substituted phenyl iodide (3 mol equiv) in anhydrous THF (10 mL), NEt_3 (1 mL) was added under N_2 gas flow. The $Pd_2(dba)_3$ (0.019 mmol) and $AsPh_3$ (0.15 mmol) were added to the mixture and the reaction mixture was stirred at 85°C for 6 h under nitrogen atmosphere. The reaction mixture was cooled at room temperature and THF was removed under reduced pressure. The crude product was purified by column chromatography (silica gel) using CH_2Cl_2: CH_3OH (1:7) as an eluent. Further purification was carried out through pre-TLC method to afford the corresponding porphyrins. Finally, the products were recrystallized in dry CH_3OH to give pure product as a green solid.

Por-C_{12}-RA_2: Yield: 50%. ^{1}HNMR (CD_3OH, 500 MHz): δ 9.51 (d, J = 4.5 Hz, 4H), 8.63 (d, J = 4.5 Hz, 4H), 8.08 (d, J = 8.45 Hz, 4H), 7.90 (d, J = 8.45 Hz, 4H), 7.60 (t, J = 8.55 Hz, 2H), 6.94 (d, J = 8.6 Hz, 4H), 3.73 (t, J = 6.1 Hz, 8H), 1.10-1.04 (m, 8H), 1.02-0.94 (m, 8H), 0.92-0.79 (m, 12H), 0.74-0.63 (m, 48H), 0.52-.049 (m, 8H), 0.22-0.17 (m, 8H). ^{13}CNMR (CD_3OH, 125 MHz): δ 174.61, 159.90, 151.51, 150.60, 132.70, 131.03, 129.55, 129.31, 123.36, 115.02, 114.56, 105.16, 100.66, 97.66, 83.35, 68.35, 31.62, 29.38, 29.35, 29.15, 29.04, 28.85, 28.53, 28.45, 25.17, 22.37, 13.15. IR: 3422 (O-H), 2923 (=C-H), 2849 (-C-H), 2192 (C≡C), 1725 (-C=O), 1568 (-C=C), 1387 (-C-O)

Por-C_{12}-RA_3: Yield: 40%. ^{1}HNMR (CD_3OH, 500 MHz): δ 9.46 (d, J = 4.5 Hz, 4H), 8.60 (d, J = 4.5 Hz, 2H), 8.58 (d, J = 4.5 Hz, 2H), 8.02 (s, 1H), 8.01 (d, J = 8.2 Hz, 4H), 7.95 (d, J = 8.1 Hz, 2H), 7.84 (d, J = 8.15 Hz, 2H), 7.59 (t, J = 8.5 Hz, 2H), 6.93 (d, J = 8.55 Hz, 4H), 3.74 (t, J = 6.0 Hz, 8H), 1.03-0.97 (m, 8H), 0.93-0.85 (m, 8H), 0.81-0.72 (m, 8H), 0.67-0.58 (m, 52H), 0.48-0.42 (m, 8H), 0.19-0.13 (m, 8H). ^{13}CNMR (CD_3OH, 125 MHz): δ 174.63, 159.83, 151.61, 151.45, 148.80, 131.33, 130.36, 130.14, 129.75 129.31, 115.26, 105.05, 99.86, 88.89, 68.25, 31.65, 29.21, 29.15, 29.08, 28.92, 28.77, 28.46, 25.16, 22.39, 13.16. IR: 3453 (O-H), 2927 (=C-H), 2847 (-C-H), 2214 (C≡N), 2191 (C≡C), 1625 (-C=O), 1583 (-C=C), 1389 (-C-O)

Por-C_8-RA_4: Yield: 50%. ^{1}HNMR (CD_3OH, 500 MHz): δ 9.49 (d, J = 4.4 Hz, 4H), 8.61 (d, J = 4.45 Hz, 4H), 8.07 (s, 2H), 8.06 (d, J = 8.35 Hz, 4H), 7.98 (d, J = 8.1 Hz, 4H), 7.55 (t, J = 8.45 Hz, 2H), 6.88 (d, J = 8.6 Hz, 4H), 3.67 (t, J = 5.25 Hz, 8H), 1.22-1.13 (m, 8H), 1.07-1.02 (m, 8H), 0.95-0.89 (m, 8H), 0.86-0.80 (m, 8H), 0.73-0.64 (m, 12H), 0.55-0.52 (m, 8H), 0.26-0.21 (m, 8H). ^{13}CNMR (CD_3OH, 125 MHz): δ 179.47, 178.04, 162.08, 155.85, 154.75, 147.54, 143.80, 133.00, 131.99, 128.41, 124.16, 123.08, 123.02, 117.09, 112.45, 109.36, 103.07, 101.67, 87.97, 85.70, 83.32, 62.15, 52.21, 30.93, 30.61, 29.35, 29.03, 22.32, 22.06, 20.70, 18.92, 17.44, 15.45, 13.07. IR: 3446 (O-H), 2916 (=C-H), 2847 (-C-H), 2217 (C≡N), 2190 (C≡C), 1635 (-C=O), 1583 (-C=C), 1362 (-C-O)

Por-C_{12}-RA_1: Yield: 70%. ^{1}HNMR (CD_3OH, 500 MHz): δ 9.42 (d, *J* = 4.4 Hz, 4H), 8.52 (d, *J* = 4.5 Hz, 4H), 8.44 (s, 2H), 7.85 (q, *J* = 7.6 Hz, 4H), 7.52 (t, *J* = 8.55 Hz, 2H), 7.35 (t, *J* = 7.5 Hz, 2H), 6.86 (d, *J* = 8.55 Hz, 4H), 3.67 (t, *J* = 5.9 Hz, 8H), 1.10-1.04 (m, 16H), 0.95-

0.87 (m, 8H), 0.83-0.77 (m, 8H), 0.73-0.65 (m, 24H), 0.60-0.56 (m, 20H), 0.52-.049 (m, 8H), 0.38-0.32 (m, 8H). ^{13}CNMR (CD_3OH, 125 MHz): δ 173.16, 159.94, 151.53, 150.55, 132.49, 131.23, 129.92, 128.62, 127.78, 114.83, 105.22, 99.59, 93.40, 68.42, 31.61, 30.60, 29.38, 29.13, 29.05, 29.03, 28.83, 28.69, 28.56, 28.47, 25.19, 22.35, 20.24, 13.12, 9.91. IR: 3448 (O-H), 2926 (=C-H), 2847 (-C-H), 2187 (C≡C), 1690 (-C=O), 1578 (-C=C), 1376 (-C-O)

Third-order NLO parameters (β, n_2, $\chi^{(3)}$, γ_h, σ_{ex} and σ_g) calculations

In the case of open aperture Z-scan, for a temporally Gaussian pulse, the transmittance can be obtained by [2-4]

$$T(z) = \frac{1}{\sqrt{\pi} q_0(z)} \int_{-\infty}^{\infty} ln\left[1 + q_0(z) e^{-\tau^2}\right] dt \qquad (1)$$

Where

$$q_0(z) = \beta I_0 \left[1 - \frac{e^{-\alpha L}}{\left(1 + \frac{z^2}{z_0^2}\right)\alpha}\right]$$

"$1 - \exp(-\alpha L)/\alpha$" is the effective length of the sample. "I_0" is the laser bean intensity at the focus and "z_0" is the Rayleigh length. For $|q_0| < 1$, this transmittance can be expressed in a more suitable form as

$$T(z) = \sum_{m=0}^{\infty} \frac{[-q_0(z)]^m}{(m+1)^{3/2}} \qquad (2)$$

In the curves, the solid line is a theoretical fit of the experimental data obtained using equation (2) which yields the value of effective third-order nonlinear absorption (TPA) coefficient "β". The open-aperture Z-scan curve display a symmetric valley with respect to the focus, which show strong nonlinear absorption for all the porphyrin samples.

In closed aperture technique, the changes in optical transmission was measured as a result of the combined nonlinear absorption and nonlinear refractive index induced phase change. The normalized transmittance in closed aperture

experiment was recorded at different sample positions and observed a prefocal peak followed by a post focal valley (Figure 2), which indicates a strong negative nonlinearity of the samples. This is due to the self defocussing effect of the laser beam within the sample. To estimate the nonlinear refractive index, the pure nonlinear refraction curve obtained by division method [4, 5] and corresponding fitting was done for on-axis nonlinear phase shift at the focus "$\Delta\Phi_0$". The nonlinear refractive index "γ (m^2/W)" can be obtained from equation 3.[6, 7]

$$\gamma = \frac{\Delta\varphi_0 \lambda}{2\pi I_0} \qquad (3)$$

And $x = z/z_0$.

The nonlinear refractive index "n_2" (esu) can be calculated from the conversion formula

$$n_2(esu) = \frac{cn_0}{40\pi}\gamma\left(m^2/W\right) \qquad (4)$$

and the third-order nonlinear susceptibility can be expressed as a complex quantity [8, 9]

$$\chi^{(3)} = \chi_R^{(3)} + i\chi_I^{(3)} \qquad (5)$$

with

$$\chi_R^{(3)} = 2n_0^2\varepsilon_0 c\gamma \qquad (6)$$

and

$$\chi_I^{(3)} = \frac{n_0\varepsilon_0 c^2\beta}{\omega} \qquad (7)$$

Where "n_0" is the linear refractive index, "ε_0" is the permittivity in vacuum, "I_0" is the irradiance of the laser beam within the sample, "c" is the speed of light in the free space and "ω" is the optical frequency. The real part "$\chi_R^{(3)}$" and imaginary part "$\chi_I^{(3)}$" articulates as the nonlinear refractive index and nonlinear absorption coefficient respectively. The nonlinear induced polarization per molecule is described by the microscopic susceptibilities known as the

hyperpolarizabilities [10] and for third order effects the corresponding hyperpolarizability "γ_h" (second order hyperpolarizability) is related to the third order susceptibility "$\chi^{(3)}$" by the equation 8

$$\gamma_h = \frac{\chi^{(3)}}{\left[(n_0^2+2)/3\right]^4 N} \qquad (8)$$

where "N" is the density of molecules in the unit of molecules per cm^3 and "n_0" is the linear refractive index of the medium.[11, 12]

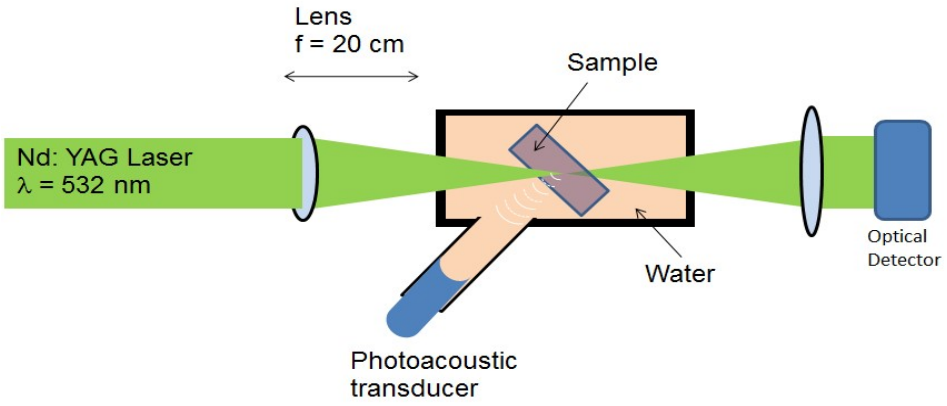

Figure S1. Schematic of experimental setup used to obtain nonlinear optical transmission data

Generally, nonlinear absorption can be caused by free carrier absorption, saturated absorption, direct multiphoton absorption or excited state absorption. A plot of nonlinear absorption coefficient versus on-axis input laser intensity helps to explore the mechanism responsible for nonlinear absorption. If the mechanism belongs to simple two photon absorption, β should be a constant independence of on axis irradiance I_0. In direct three photon absorption mechanism, β should be a linear increasing function of I_0 and the intercepts on vertical axis should be non-zero [13]. Reverse saturation absorption occurs in a molecule when excited state cross-section is larger than the ground state cross-section [14, 15]. For all the samples we observed that β is decreasing with increasing with I_0. The fall of β with an increase of I_0 can be observed for instantaneous saturation of absorption (SA) if $\sigma_{ex}<\sigma_{\gamma}$. [15]

The excited state absorption cross-section (σ_{ex}) was measured from the open-aperture Z-scan data. The change in the intensity of the laser beam as it propagates through the sample is given by

$$\frac{dI}{dz} = -\alpha I - \sigma_{ex} N(t) I \qquad \text{and} \qquad \frac{dN}{dt} = \frac{\sigma_{ex} I}{\hbar\omega} \qquad (9)$$

where "I" is the intensity, "z" is the sample position, "N" is the density of charges in the excited state, "ω" is the angular frequency of the laser and "α" is the linear absorption coefficient. From equation 3, $q_0 = \sigma_{ex}\alpha F_0 L_{eff}/2h\nu$ where "F_0" is the fluence of the laser at the focus. A proper fit of the open-aperture data with the equation gives the values of excited state absorption cross-section (σ_{ex}). The ground state absorption cross-section, σ_g can be calculated from the equation, $\alpha = \sigma_g N_a C$; where "N_a" is the Avogadro's number and "C" is the concentration.

TGA measurements

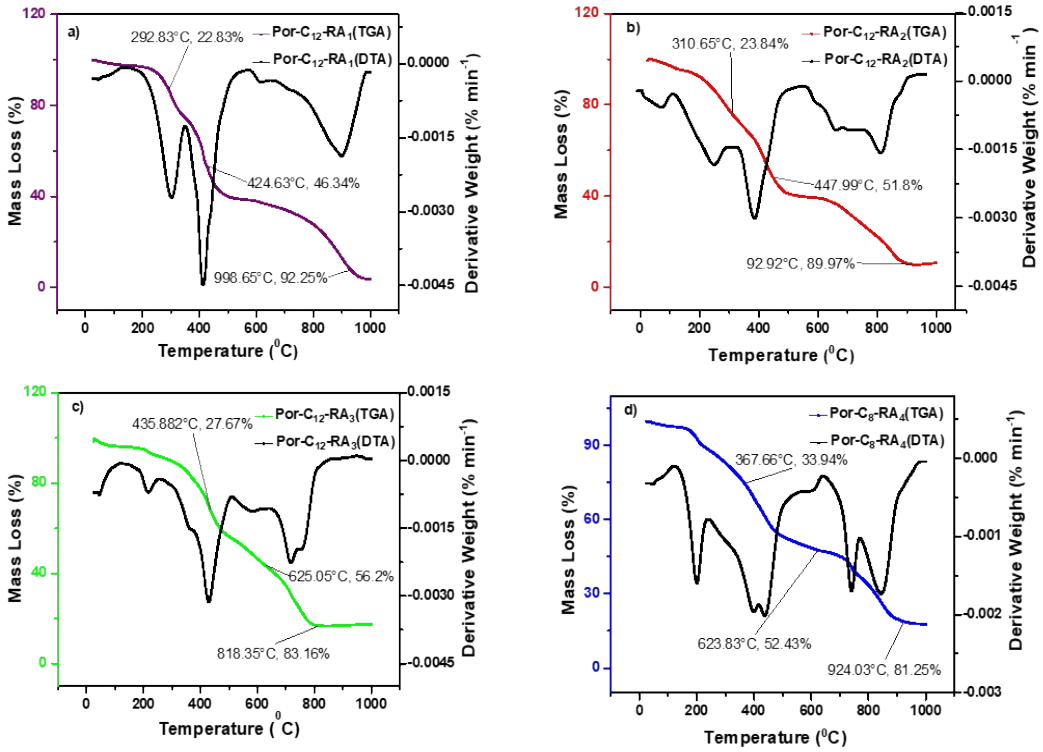

Figure S2. TGA curve of (a) Por-C_{12}-RA_1; (b) Por-C_{12}-RA_2; (c) Por-C_{12}-RA_3 and (d) Por-C_8-RA_4

Figure S2 shows the TGA curves for all the samples. It is revealed that the TG curves of all the complexes show a continuous weight loss starting from 150 °C to 990 °C, until stable ZnO oxides are formed at around 950 °C or above. The initial weight loss of about 22.83%, 23.84%, 27.67% and 33.94% observed between 200 °C and 450 °C for Por-C_{12}-RA_1, Por-C_{12}-RA_2, Por-C_{12}-RA_3 and Por-C_8-RA_4 respectively, are attributed to the removal of ethnyl-phenyl rings. At 450 °C–550 °C, up to 50% of the total weights had been lost which correspond to the loss of alkoxy-phenyl groups. The organic moiety decomposes further with increasing temperature. At around 410 °C–4450 °C, up to 70% of the total mass had been lost; correspondingly there is a large peak in DTA

curves attributed to the collapse of macrocyclic ligand. Further in the range of 500 °C–950 °C, the weight losses reach up to 97% which are attributed to the removal of pyrrole groups and complete decomposition of macrocyclic rings finally leaving behind zinc oxide. Simultaneously, there are some peaks in 200 °C–950 °C region in the DTA curves indicating the major loss in this region. The small peaks correspond to the loss of substituents on porphyrin ring and the large peaks correspond to the collapse of the porphyrin skeleton.

FTIR measurements

The Fourier transform infrared absorption spectra of Por-C_n-RA_m porphyrins were acquired by using a Perkin-Elmer 580B spectrophotometer, equipped with a Perkin-Elmer 3600 IR data station, in KBr pellets. All the samples were flushed with N_2 gas before measurements and the IR spectra were recorded at spectral range between 700 and 4000 cm^{-1}. Baseline spectra were obtained using KBr pellet only under the same conditions. The Experimental IR for all the synthesized porphyrin are shown in Figure S3.

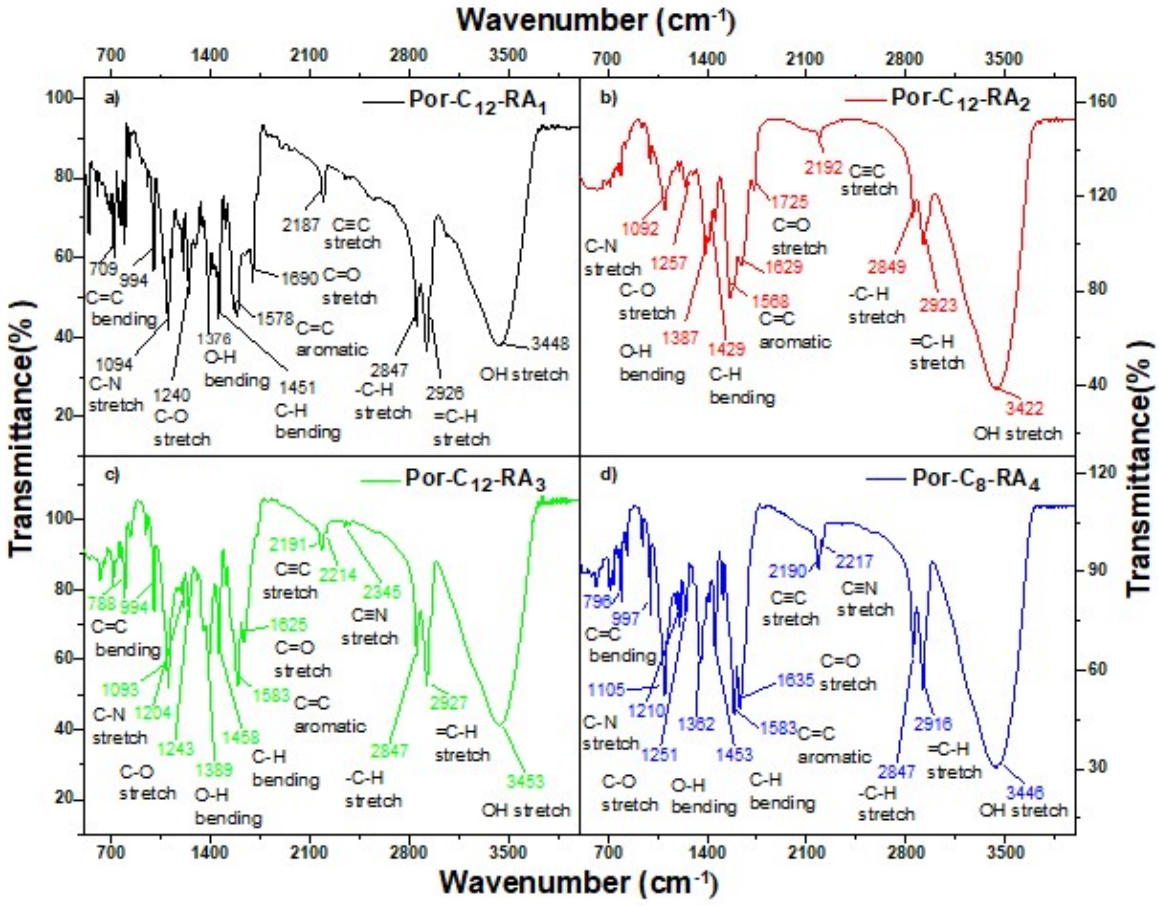

Figure S3. Experimental FTIR spectra of (a) Por-C_{12}-RA_1; (b) Por-C_{12}-RA_2; (c) Por-C_{12}-RA_3 and (d) Por-C_8-RA_4

NMR spectra

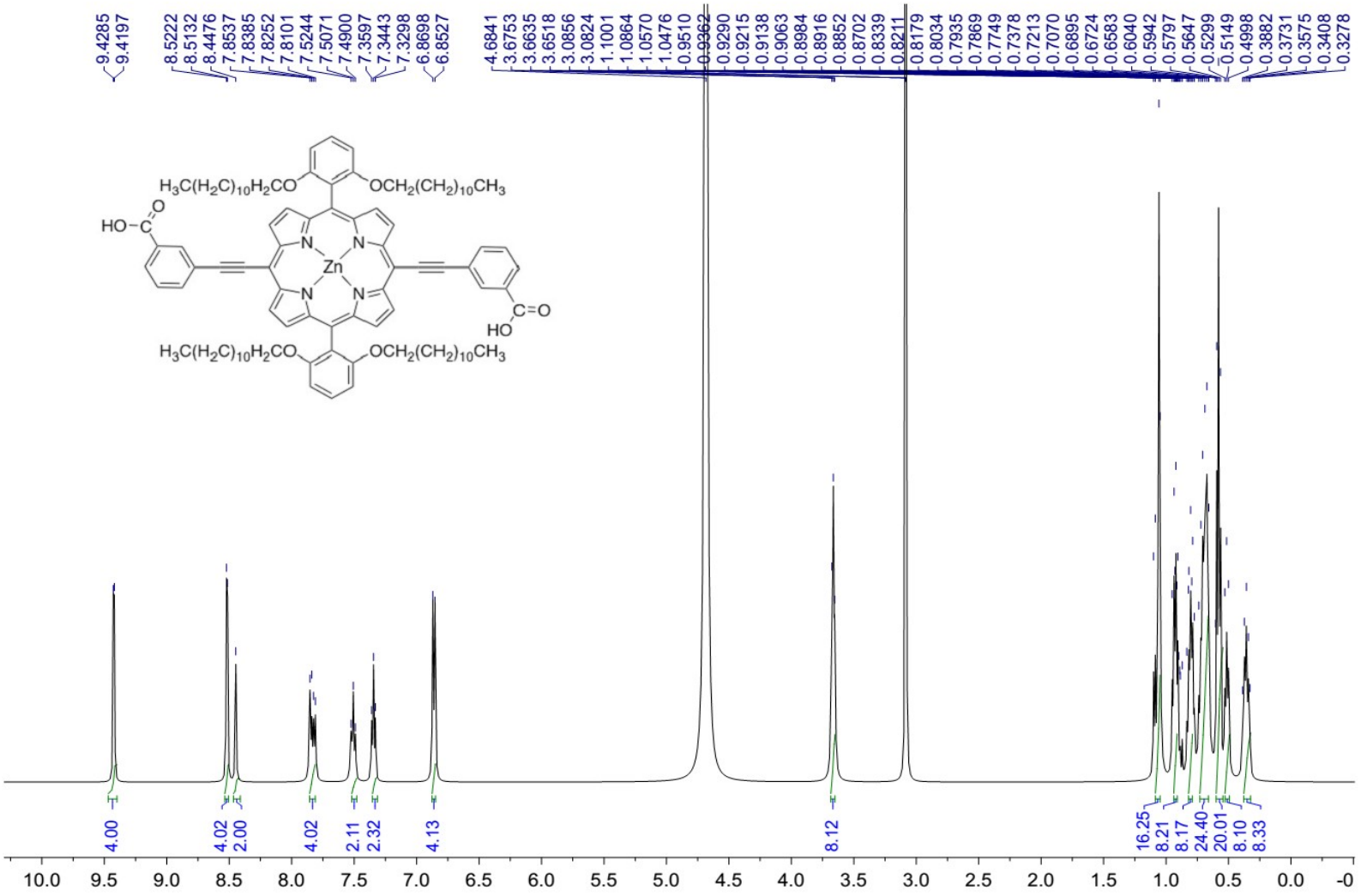

Figure S4. ^{1}HNMR of [5,15-bis(2,6-di(dodecyloxy)phenyl)-10,20-bis(3-carboxylphenyl)ethynyl)porphinato]zinc(II) (Por-C_{12}-RA_1) in CD_3OH

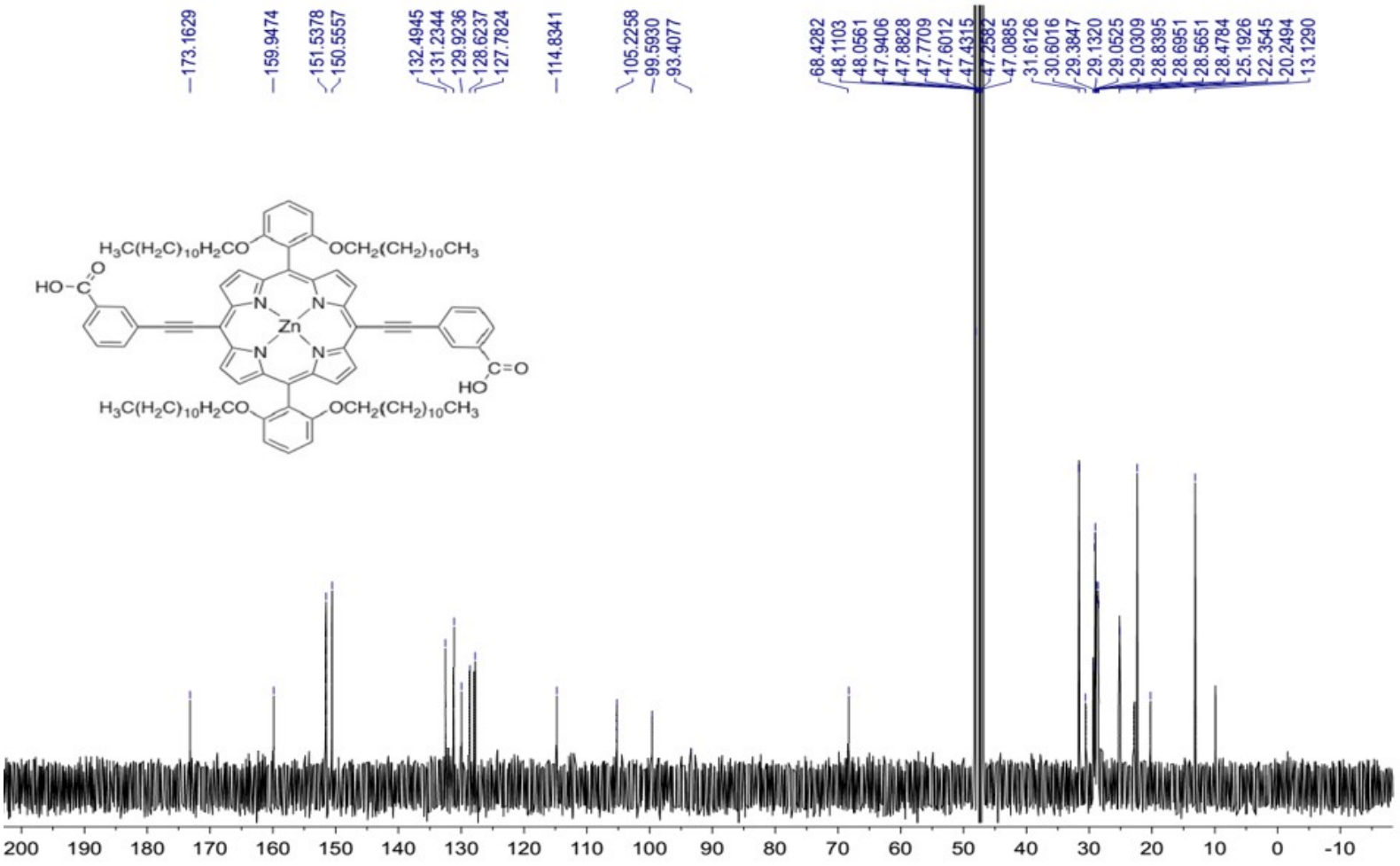

Figure S5. ^{13}CNMR of [5,15-bis(2,6-di(dodecyloxy)phenyl-10,20-bis(3-carboxylphenyl)ethynyl)porphinato]zinc(II) (Por-C_{12}-RA_1) in CD_3OH

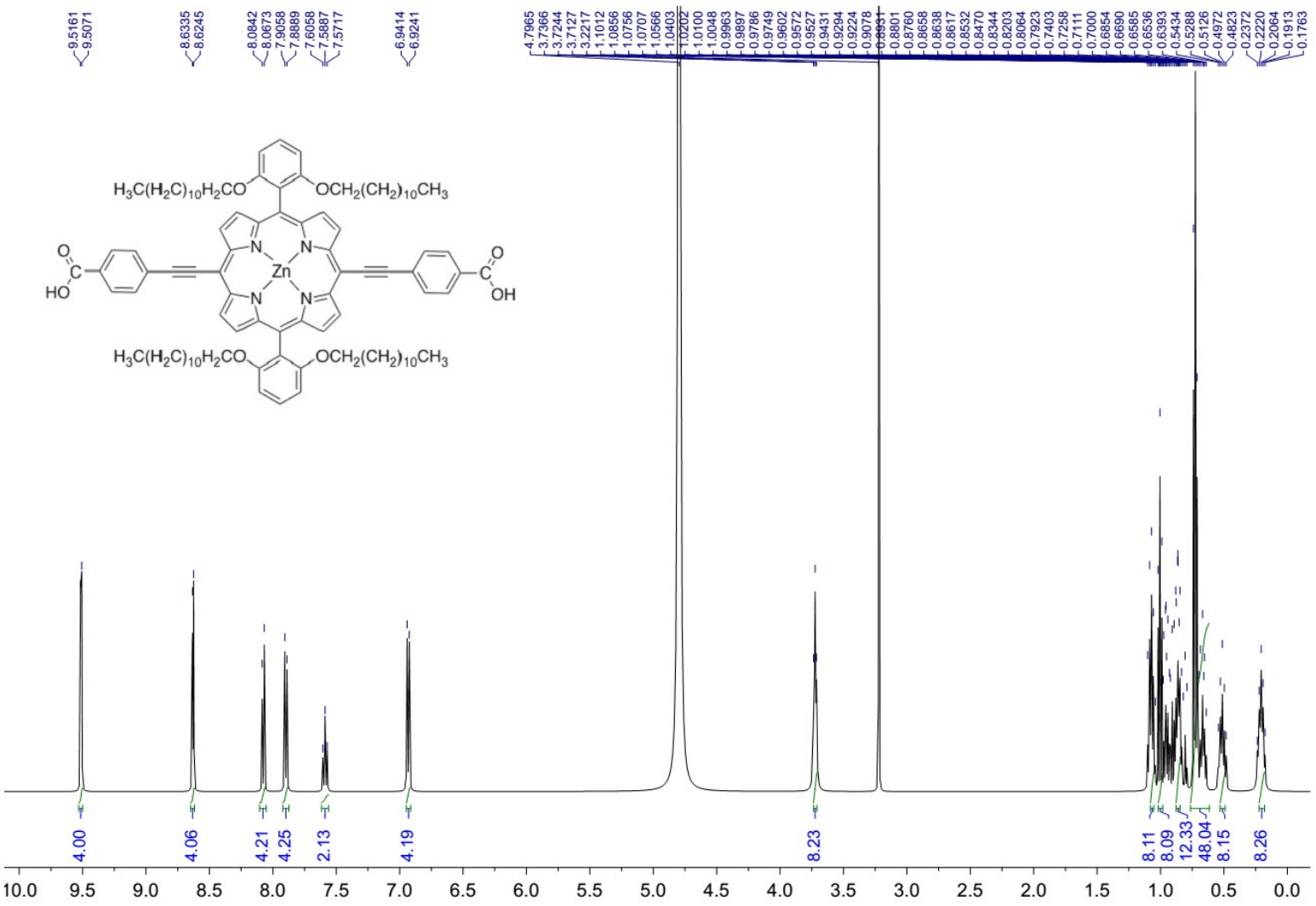

Figure S6. ^{1}HNMR of [5,15-bis(2,6-di(dodecyloxy)phenyl)-10,20-bis(4-carboxylphenyl)ethynyl)porphyrinato]zinc(II) (Por-C_{12}-RA_2) in CD_3OH

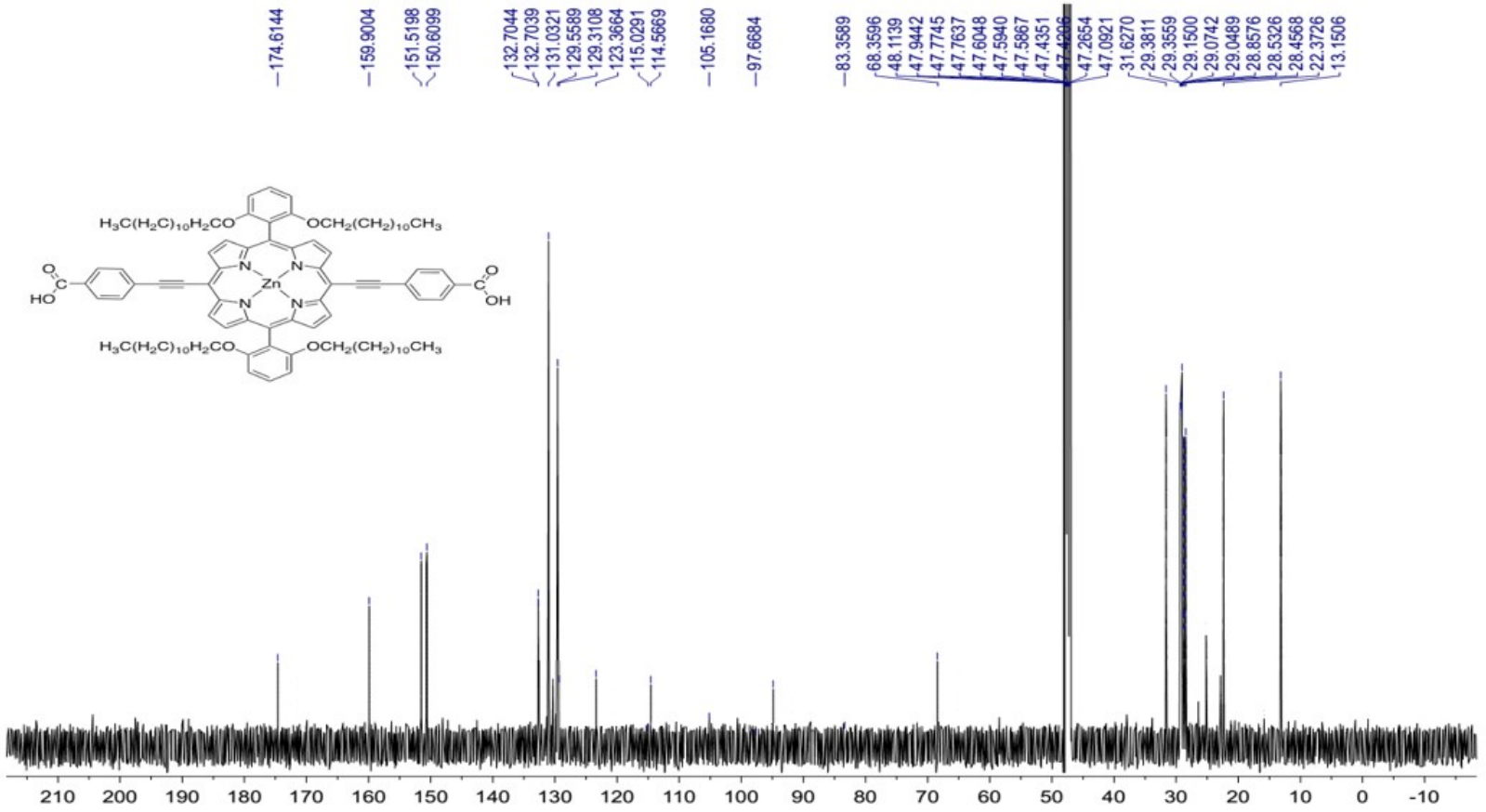

Figure S7. ^{13}CNMR of [5,15-bis(2,6-di(dodecyloxy)phenyl-10,20-bis(4-carboxylphenyl)ethynyl)porphyrinato]zinc(II) (Por-C_{12}-RA_2) in CD_3OH

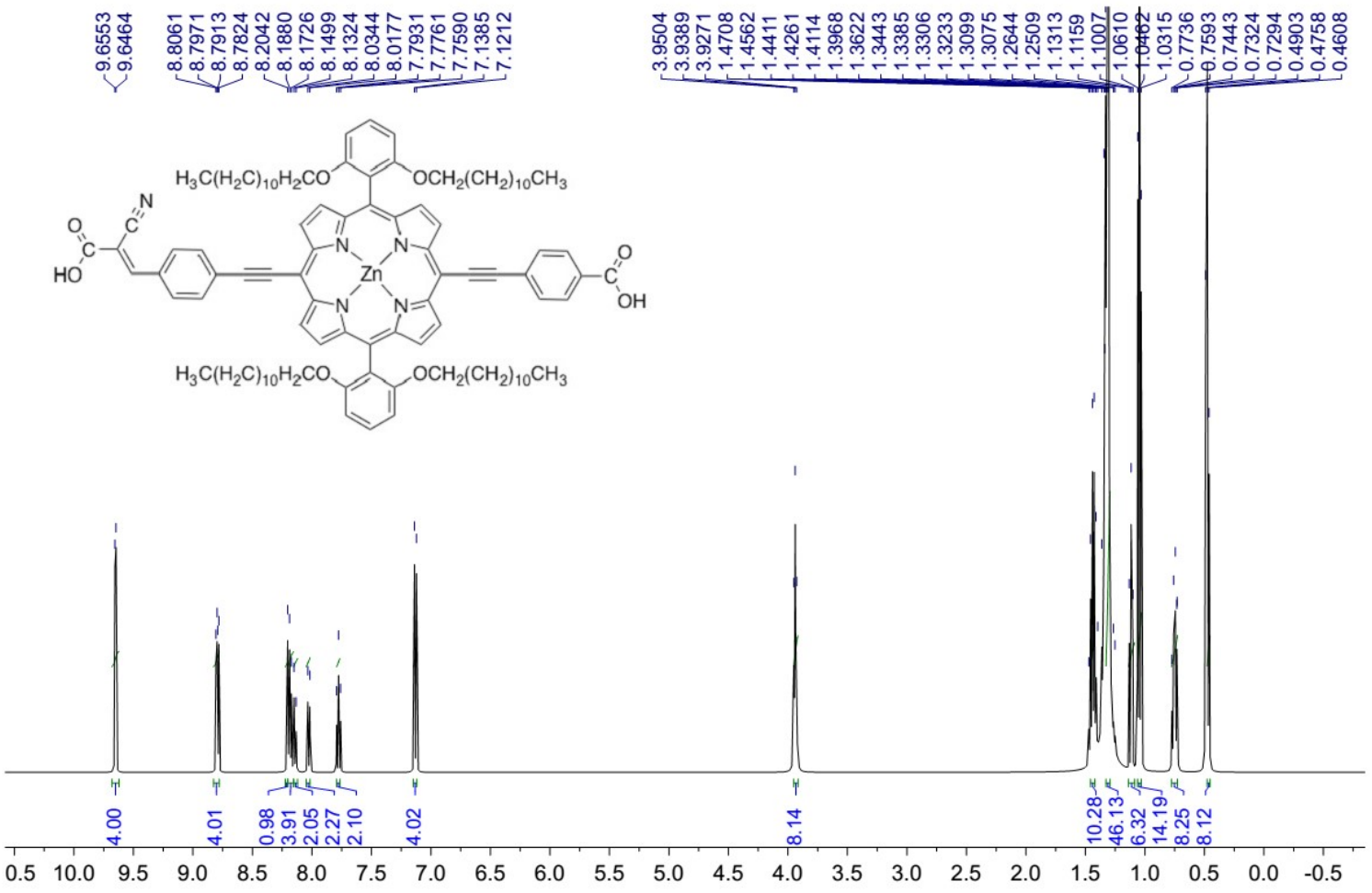

Figure S8. ^{1}HNMR of [5,15-bis(2,6-di(dodecyloxy)phenyl)-10-[(4-carboxylphenyl)ethynyl]-20-[(4-(2-cyanopropenoicacid)phenyl)ethynyl] porphyrinato]zinc(II) (Por-C_{12}-RA_3) in CD_3OH

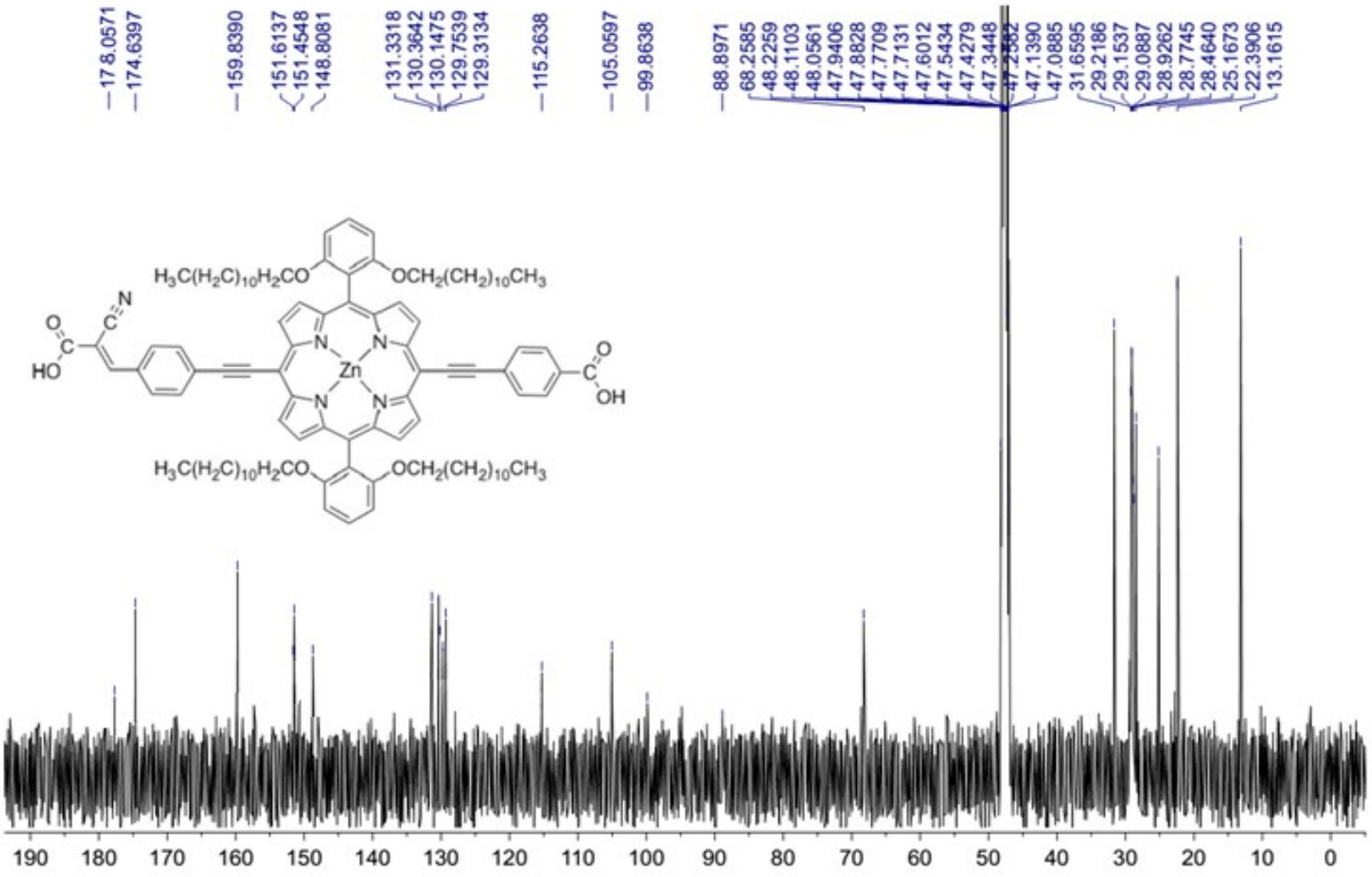

Figure S9. ^{13}CNMR of [5,15-bis(2,6-di(dodecyloxy)phenyl)-10-[(4-carboxylphenyl)ethynyl]-20-[(4-(2-cyanopropenoicacid)phenyl)ethynyl] porphyrinato]zinc(II) (Por-C_{12}-RA_3) in CD_3O

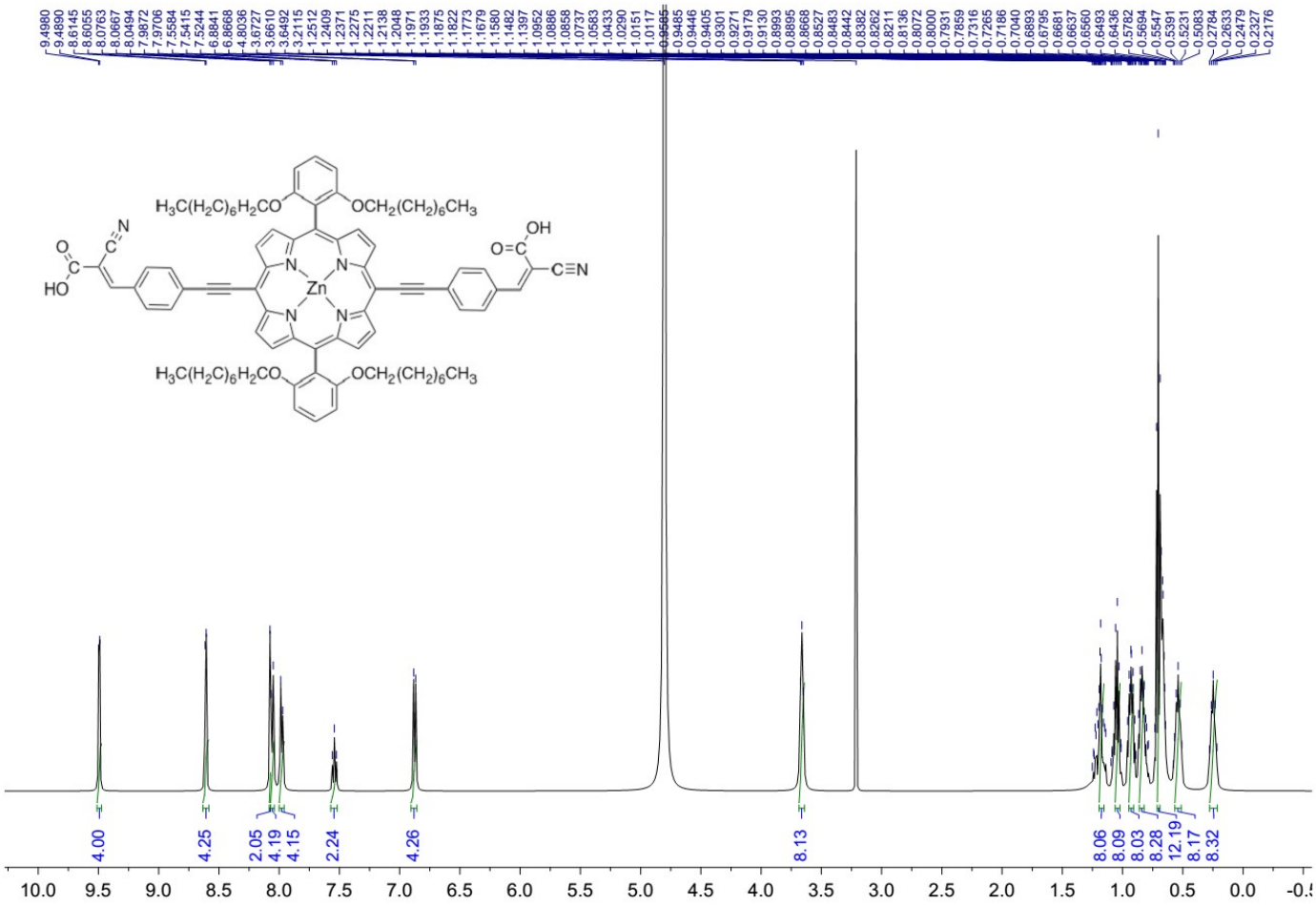

Figure S10. [1]HNMR of [5,15-bis(2,6-di(octyloxy)phenyl)-10,20-[(4-(2-cyanopropenoicacid)phenyl)ethynyl]porphyrinato]zinc(II) (Por-C_8-RA_4) in CD_3OH

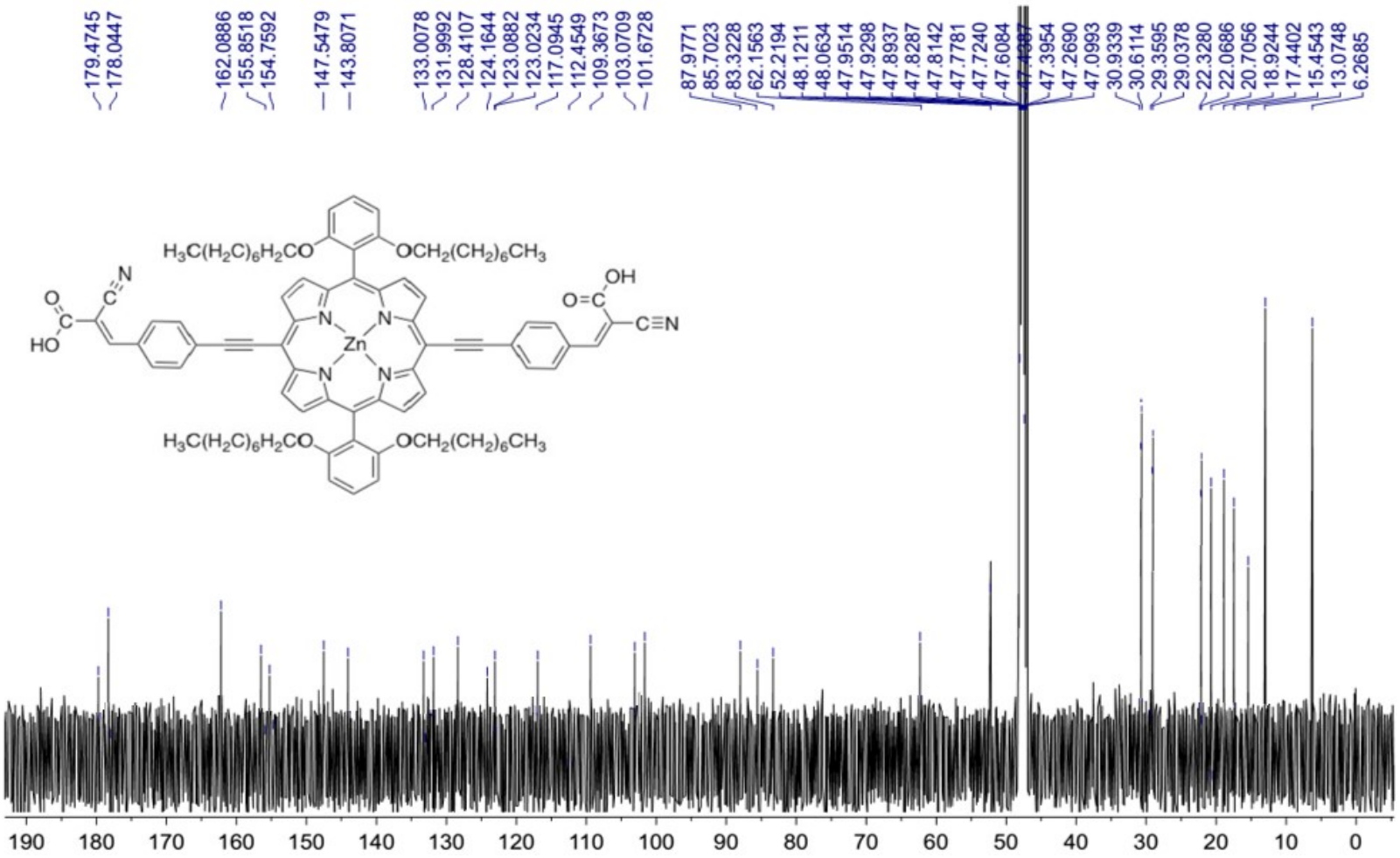

Figure S11. ^{13}CNMR of [5,15-bis(2,6-di(octyloxy)phenyl)-10,20-[(4-(2-cyanopropenoicacid)phenyl)ethynyl]porphyrinato]zinc(II) (Por-C_8-RA_4) in CD_3OH

References

1. A. Yasin, V. S. Nair, S. A. Aravindh, S. M. Sarkar, M. Hatamimoslehabadi, S. Mitra, M. H. Ab Rahim, J. La, I. S. Roqan, M. M. Yusoff, C. S. Yelleswarapu and R. Jose, *Journal of Materials Chemistry C*, 2020, **8**, 8546-8559.
2. M. Sheik-Bahae, A. A. Said and E. W. Van Stryland, *Optics letters*, 1989, **14**, 955-957.
3. C. S. Yelleswarapu and S.-R. Kothapalli, *Optics express*, 2010, **18**, 9020-9025.
4. M. SHEIK-BAHAE, A. A. SAID, T.-H. WEI, D. J. HAGAN and E. Van Stryland, *SPIE milestone series*, 2003, **174**, 292-301.
5. P. Chapple, J. Staromlynska, J. Hermann, T. Mckay and R. McDuff, *Journal of Nonlinear Optical Physics & Materials*, 1997, **6**, 251-293.
6. F. Zhao, C. Wang, J. Zhang and Y. Zeng, *Optics Express*, 2012, **20**, 26845-26851.
7. F. Qiu, D. Yang, P. Li and X. Wang, *Express Polymer Letters*, 2008, **2**, 823-828.
8. L. Brzozowski and E. H. Sargent, *Journal of Materials Science: Materials in Electronics*, 2001, **12**, 483-489.
9. H. El Ouazzani, K. Iliopoulos, M. Pranaitis, O. Krupka, V. Smokal, A. Kolendo and B. Sahraoui, *The Journal of Physical Chemistry B*, 2011, **115**, 1944-1949.
10. H. S. Nalwa and S. Miyata, *Nonlinear optics of organic molecules and polymers*, CRC press, 1996.
11. P. Paufler, *Crystal Research and Technology*, 1991, **26**, 802-802.
12. W. Feng, W. Yi, H. Wu, M. Ozaki and K. Yoshino, *Journal of applied physics*, 2005, **98**, 034301.
13. A. J. Kiran, K. Chandrasekharan, S. R. Nooji, H. Shashikala, G. Umesh and B. Kalluraya, *Chemical physics*, 2006, **324**, 699-704.
14. R. L. Sutherland, *Handbook of nonlinear optics*, CRC press, 2003.
15. S. Couris, E. Koudoumas, A. Ruth and S. Leach, *Journal of Physics B: Atomic, Molecular and Optical Physics*, 1995, **28**, 4537.